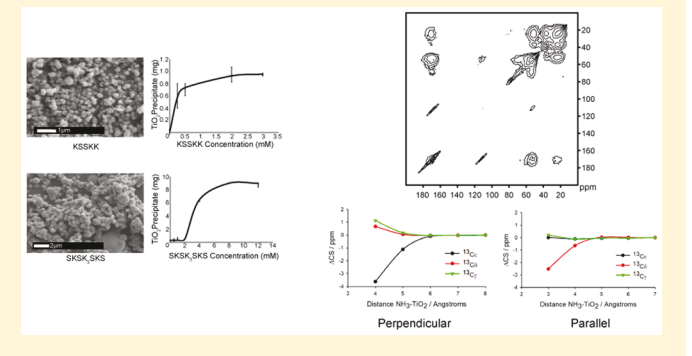


Serine—Lysine Peptides as Mediators for the Production of Titanium Dioxide: Investigating the Effects of Primary and Secondary Structures Using Solid-State NMR Spectroscopy and DFT Calculations

Erika L. Buckle,[†] June S. Lum,[‡] Adrienne M. Roehrich,[†] Robert E. Stote,[‡] Branden Vandermoon,[†] Martin Dracinsky,*,* Shaun F. Filocamo,[‡] and Gary P. Drobny[†]

Supporting Information

ABSTRACT: A biomimetic approach to the formation of titania (TiO₂) nanostructures is desirable because of the mild conditions required in this form of production. We have identified a series of serine-lysine peptides as candidates for the biomimetic production of TiO2 nanostructures. We have assayed these peptides for TiO2-precipitating activity upon exposure to titanium bis(ammonium lactato)dihydroxide and have characterized the resulting coprecipitates using scanning electron microscopy. A subset of these assayed peptides efficiently facilitates the production of TiO₂ nanospheres. Here, we investigate the process of TiO2 nanosphere formation mediated by the S-K peptides KSSKK- and



SKSK₃SKS using one-dimensional and two-dimensional solid-state NMR (ssNMR) on peptide samples with uniformly ¹³Cenriched residues. ssNMR is used to assign ¹³C chemical shifts (CSs) site-specifically in each free peptide and TiO₂-embedded peptide, which are used to derive secondary structures in the neat and TiO₂ coprecipitated states. The backbone ¹³C CSs are used to assess secondary structural changes undergone during the coprecipitation process. Side-chain ¹³C CS changes are analyzed with density functional theory calculations and used to determine side-chain conformational changes that occur upon coprecipitation with TiO₂ and to determine surface orientation of lysine side chains in TiO₂-peptide composites.

INTRODUCTION

Titanium(IV) oxide (titania, TiO₂) is used in the production of pigments, insulators, photocatalysts, and textile coatings and in pathogenic detection and chemical decontamination. 1-12 Synthetic methods with fine-tuned control over particle size, crystallinity, and morphology are necessary because these applications require unique physical properties for TiO₂. ¹³ This is a significant caveat because many current methods of production require extreme temperature, pressure, and pH, while lacking the desired level of control over crystallinity and morphology. 14-18 As a result, efforts have been focused on exploring biomimetic, peptide-mediated syntheses that produce TiO₂ with consistent morphologies. 19-22

Biological organisms can produce inorganic materials composed of calcite, silica, and hydroxyapatite through a process known as biomineralization. These organisms contain specialized proteins, which, together with a variety of organic molecules, direct hard tissue formation, yielding highly structured forms under ambient conditions. Biosilica, the most abundant biomineral, is predominately produced by the diatom, a marine algae which takes in silicon in the form of

silicic acid (Si(OH)₄) and catalyzes its deposition as silica (SiO_2) . $^{21,23-27}$ The protein implicated in regulating the process of SiO₂ biomineralization in the marine diatom Cylindrotheca fusiformis is silaffin Sil1p.²⁴ The primary structure of Sil1p has a repetitive sequence between residues 108 and 271, composed of seven units, the fifth of which is a 19 amino acid peptide called R5 (SSKKSGSYSGSKGSKRRIL). R5 precipitates SiO₂ nanospheres in vitro in a manner similar to Sil1p without the need for Sil1p's many posttranslational modifications. 28,29 While some silaffins and segments thereof have low sequence homology, R5 is rich in both serine and lysine residues, which are essential to R5's silica-precipitating activity in vitro. $^{30-32}$

Kroger and co-workers have identified lysine-rich motifs conserved in many silaffins. When examining the silaffin Sil3 from Thalassiosira pseudonana, they found peptide segments in both the N-terminal and C-terminal domains that exhibit a high density of five lysine residues, all with similar spacing.³³ These

Received: January 22, 2018 Revised: March 28, 2018 Published: March 29, 2018

[†]Department of Chemistry, University of Washington, Box 351700, Seattle, Washington 98195, United States

[‡]Biological Sciences and Technology Team, US Army Natick Soldier Research, Development and Engineering Center, Natick, Massachusetts 01760, United States

[§]Institute of Organic Chemistry and Biochemistry, Czech Academy of Sciences, Flemingovo 2, 16610 Prague, Czech Republic

peptides follow the sequence $KxxKxxK_yKxxK$, where y = 1-3 residues, and are referred to as pentalysine clusters. The remaining silaffins (Sil1, Sil2, and Sil4) of T. pseudonana also contain pentalysine clusters. Through extensive mutation studies, Kröger found that PLC1, a pentalysine cluster from Sil1, exhibited efficient silica-targeting activity. PLC1 has a higher number of hydroxylated residues than other mutants with lower silica-targeting activity, which is corroborated by the activity of T6, a highly efficient silica-targeting peptide rich in serine. They designed an artificial pentalysine cluster PLCart (KSSKSSKSSKSSK), which also demonstrates silica-targeting efficiency. 33

Goobes and co-workers precipitated silica in vitro using PL12 (KAAKLFKPKASK), a pentalysine cluster from Sil3. They examined the secondary structure of PL12 using dynamic nuclear polarization magic-angle spinning (DNP MAS) NMR and found that PL12 is mostly unstructured. They used CS differences between the neat and SiO₂-embedded peptide to discern changes in the backbone structure and side-chain—SiO₂ interactions. A close interaction between lysine side chains and the SiO₂ surface was further supported by two-dimensional (2D) ^{1}H — ^{29}Si HETCOR measurements, which indicate that the $^{1}\text{H}\varepsilon$ are in contact with Q⁴ silicon sites. They was a supported by the side of the si

In addition to silaffins and their peptide fragments, many silicification methods involve the use of poly-L-lysine chains, ^{35,36} polyamines, ^{23,37–39} peptides rich in amino groups, or amphiphilic peptides rich in lysines, such as LK α 14. ^{40–42} The results of these varied silicification procedures indicate the importance of lysine residues in these processes.

Biomimetic approaches are being applied to the production of other oxides, with a specific emphasis on ${\rm TiO_2}$. $^{19,21,38,43-50}$ Many of these methods include the use of lysine-rich peptides or small organic amines and have shown the importance of clusters of lysine (and arginine) residues in these ${\rm SiO_2}$ - and ${\rm TiO_2}$ -precipitating systems. 30,31,51,52

Here, we investigate the effects of primary structure of serine-lysine (S-K) peptides on TiO₂ precipitation. The relative numbers of S and K residues within the primary sequence result in TiO2 of varied size and morphology. To understand how these S-K peptides direct the formation of specific TiO2 morphologies, we pair a molecular-level solidstate NMR (ssNMR) investigation of the peptide structure with the resultant TiO2 morphology and precipitation isotherm studies. We use an iterative process in which the peptide sequences are modified and the resulting morphologies are determined followed by ssNMR to characterize the structures of a selection of the S-K peptides both in their neat form and within the TiO₂ coprecipitate. We use ¹³C cross-polarization magic-angle spinning (CP MAS) in one-dimensional (1D) and 2D experiments, allowing for the assignment of chemical shifts (CSs) to backbone and side-chain ¹³C spins. The CS data is input into TALOS-N,52 which predicts torsion angles and thus provides secondary structures for these selected peptides. A comparison of CS data and secondary structure differences provides information on whether TiO2 coprecipitation induces any changes in the peptides while also providing information on the proximity of the side chains to the TiO2 surface. The latter properties are determined from the changes in lysine side chain 13C CSs observed upon precipitation with TiO2 and quantified using density functional theory (DFT) calculations. The structural forms and interactions of S-K peptides in TiO₂ composites with spherical morphology are compared to the

corresponding properties of peptides in biosilica composites with a similar morphology.

■ EXPERIMENTAL SECTION

Materials. Trizma hydrochloride (Tris HCl) and titanium-(IV)bis(ammonium lactato)dihydroxide (TiBALDH, 50 wt % in water) were purchased from Sigma-Aldrich (St. Louis, MO) and used as received. Tiron reagent was purchased from Fisher Scientific (Waltham, MA). When purchased, S-K peptides were custom-made and supplied at >85% purity by New England Peptide, LLC (Gardner, MA). A Thermo Scientific Megafuge 40R Centrifuge (equipped with BIOLiner microplate holders) at 4 °C for 30 min was used in quantification procedures. An EON microplate reader (BioTek U.S., Winooski, Vermont) was utilized to measure the absorbance values. All natural and uniformly labeled ¹³C amino acids were purchased from Sigma-Aldrich (St. Louis, MO). Preloaded 9fluorenylmethoxycarbonyl (FMOC)-protected Wang resin was purchased from EMD Millipore (Billerica, MA). All other reagents were purchased from Sigma-Aldrich (St. Louis, MO) and used without purification.

Peptide Synthesis. Peptides were either purchased from New England Peptide or synthesized on a CEM Liberty Blue peptide synthesizer using a standard FMOC and *tert*-butyl protection scheme. Preloaded FMOC-protected Wang resin was used for solid phase synthesis. Peptides were cleaved from the resin in a 10 mL solution of 95:2.5:2.5 trifluoroacetic acid/triisopropylsilane/water per 1.0 g of peptide/resin. The resulting filtrate was added dropwise to cold *tert*-butyl methyl ether, followed by centrifugation and three rinses with 40 mL of cold *tert*-butyl methyl ether. Peptides were then dissolved in Millipore water and lyophilized, resulting in pure peptide.

TiO₂ Assay. TiBALDH (15 μ L, 1 v/v %) was added to a solution of 15 μL of S–K peptide (final concentration of 1 mg/ mL) in 45 μ L of 25 mM Tris buffer, pH 7.2 (the final solution volume in the microplate well is 75 μ L). The solution was incubated for 23 h, upon which 75 μ L of Tris buffer was added to double the volume (for quantification only), and the solution was incubated for an additional hour. The microplates were spun down for 30 min at 4 $^{\circ}$ C, and 20 μ L of the supernatant was removed from each well three times. The supernatant solutions were added to 180 µL of 5 mM Tiron reagent prepared with 1 M sodium acetate buffer, pH 4.7. Ti^{IV} depletion was monitored for 60 min, visualized by the formation of a yellow complex between Ti^{IV} and Tiron. 53,54 Solutions were equilibrated for 1 h before absorbance values were measured at 380 nm using an EON microplate reader (BioTek U.S., Winooski, Vermont). Data are a mean from three independent repeats.

KSSKK-TiO₂ Precipitation. TiBALDH (1 M, 0.2% by volume) was added to a solution of peptide (1 mg/mL) dissolved in 25 mM Tris buffer, pH = 7.2, and agitated for 24 h. After centrifugation at 2500 rpm for 10 min, the solution was decanted. The resulting precipitate was rinsed with Millipore water three times and dried in vacuo.

SKSK₃**SKS-TiO**₂ **Precipitation.** TiBALDH (1 M, 10% by volume) was added to a solution of peptide (20 mg/mL) dissolved in 25 mM TRIS buffer, pH = 7.2, and agitated for 24 h. After centrifugation at 2500 rpm for 10 min, the solution was decanted. The resulting precipitate was rinsed with Millipore water three times and dried in vacuo.

Nanoparticle Characterization. SEM images were taken on a FEI Sirion XL30 scanning electron microscope operating

at variable voltages. Precipitates were dispersed onto carbon tape, mounted on aluminum studs, and sputter-coated for 60 s with Au/Pd.

Solid-State NMR. All ssNMR experiments were conducted using a 16.44 T magnetic field (proton resonant field of 700.18 MHz) on a Bruker AVANCE III spectrometer fitted with a 1 H $\{^{13}$ C, 15 N $\}$ 3.2 mm MAS probe. The 13 C NMR signal was enhanced using CP with a 1 H $^{-13}$ C contact time of 1.1 ms. A MAS rate of 10 kHz \pm 5 Hz was maintained with a Bruker MAS controller unit. One dimensional 13 C CPMAS experiments were performed with a proton 90 time of 2.75 μ s and a recycle delay of 2 s. The number of scans for the neat and TiO $_2$ complex ranged from 2k to 16k. DARR 55 experiments were run with 60 ms mixing times and a recycle delay of 1.5 s, with 2048 slices in the F2 dimension and 512 in F1. All CSs reported were indirectly referenced to tetramethylsilane in the solid-state using adamantane (δ = 38.48). 56

DFT Calculations. The geometry of protonated *N*-acetyl-L-lysine-methylamide was optimized at the DFT level of theory, using B3LYP functional^{57,58} and a standard 6-31+G(d,p) basis set. The NMR parameters were calculated using the GIAO method with the polarizable continuum model used for implicit water solvation. ^{59,60} The Gaussian16 program package was used throughout this study. ⁶¹

To estimate the effect of side-chain conformation on carbon CSs, the conformation of compound ${\bf 1}$ was systematically modified from all-trans conformation to a conformer with a selected C-C-C-C or C-C-C-N torsion angle changed to + or -gauche conformation and the geometry of the resulting structure was optimized and NMR parameters were calculated at the same computational level as described above.

A model of the ${\rm TiO_2}$ surface was based on the anatase structure. A cluster of 6 Ti atoms and 18 O atoms was cut out of the structure and 9 hydrogen atoms were put on dangling oxygen atoms on the "inner face" of the cluster and no hydrogen atoms were put on three "surface face" oxygens, leaving the total charge of the cluster -3.

RESULTS

Effects of the Primary Structure on TiO₂ Precipitation.

We explored the effects of the K–S ratio and contiguity of K residues on TiO₂ precipitation activity. We designed a series of S–K peptides and studied their TiO₂ precipitation activity. The array was designed to test the impact of (1) an increasing number of lysine residues with a constant number of serine residues and (2) the number of contiguous lysine residues, achieved by changing the position of the serine residues. Ti^V depletion was monitored for 60 min using a colorimetric assay, visualized by the formation of a yellow complex between Ti^{IV} and Tiron. ^{53,54} Absorbance values were measured at 380 nm and used to determine the percentage of reacted Ti^{IV}. The results of the TiO₂ precipitation assays are summarized in Table 1, along with the resultant morphologies determined via SEM (images not shown).

Table 1. Peptide Sequences with Their Percentage of Reacted TiBALDH and Resultant TiO₂ Morphologies upon Coprecipitation

peptide	K—S ratio	contiguous K residues	% TiBALDH reacted (SD)	${ m TiO_2}$ morphology
SKSK ₃ SKS	1.25	3	97 (1)	spheres
KSSKK	1.5	2	22 (5)	spheres
$(SKSK_3)_2$	2	3	49 (22)	fused particles
$(SK_4S)_2$	2	4	34 (13)	amorphous
K ₃ SKSK ₃	3.5	3, 3	42 (18)	fused particles
SK ₈ S	4	8	74 (2)	fused particles
S_2K_8	4	8	73 (4)	fused particles
S_2K_9	4.5	9	38 (14)	amorphous
SK ₉ S	4.5	9	44 (16)	amorphous
SK ₅ SK ₄	4.5	5, 4	39 (15)	amorphous
SK_2SK_7	4.5	2, 7	57 (21)	amorphous
SKSK ₉	5	9	44 (17)	fused particles
SK ₅ SK ₅	5	5, 5	57 (19)	spheres

With the exception of SKSK₃SKS, peptides with a higher K–S ratio show greater TiO₂ precipitation activity, especially when the K residues are localized (i.e. SK₈S). SKSK₃SKS seems to be an anomaly as the most efficient peptide tested, converting 97% of TiBALDH into TiO₂. Only three of the peptides assayed, KSSKK, SK₅SK₅, and SKSK₃SKS, produce consistent spherical morphologies, making them of special interest. We have further investigated two of these peptides, SKSK₃SKS and KSSKK, both of which form spherical morphologies but display the highest and lowest percentages of TiBALDH reacted, respectively.

Figure 1 shows an SEM image of the KSSKK-TiO₂ coprecipitate (Figure 1a) and a corresponding size distribution histogram (Figure 1b). The coprecipitates are approximately spherical with a mean diameter of 201 \pm 46 nm. The SKSK₃SKS-TiO₂ coprecipitates are also approximately spherical (Figure 1d) but have a mean diameter of 511 \pm 202 nm, on average 300 nm larger than the KSSKK-TiO₂ nanostructures. Although many of the SKSK₃SKS-TiO₂ particles fall within a size range of 400–600 nm (Figure 1e), the nanospheres are relatively polydisperse in comparison to those of the KSSKK-TiO₂ coprecipitates.

Precipitation curves were also obtained for varying concentrations of KSSKK and SKSK₃SKS, with TiBALDH held at constant concentrations of 2 mM and 0.1 M, respectively. These precipitation curves are shown in Figure 1c,e. A striking feature of these data is that the precipitation curves have markedly different forms. The KSSKK precipitation curve in Figure 1c has a roughly hyperbolic form with the TiO₂ precipitate appearing at relatively low concentrations of peptide. In contrast, the SKSK₃SKS data in Figure 1e appear to follow sigmoidal behavior with little or no precipitate appearing until the peptide concentration reaches 2 mM and then rises rapidly. Hyperbolic and sigmoidal precipitation curves are generally attributed to noncooperative and cooperative mechanisms, respectively. We will discuss these data further below.

¹³C CS Assignments and Secondary Structure Analysis of SKSK₃SKS-Neat and SKSK₃SKS-TiO₂. In order to gain insights into the secondary structure of SKSK₃SKS-neat and

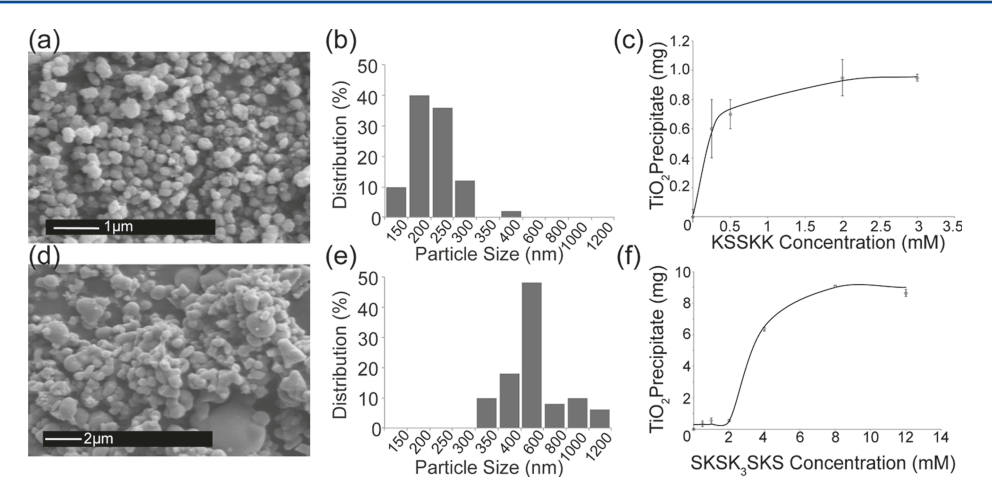


Figure 1. (a) SEM image of KSSKK-TiO₂ coprecipitates showing spherical morphologies with a mean diameter of 201 ± 46 nm. (b) Size distribution histogram for KSSKK-TiO₂ coprecipitates. Particle sizes are measured using ImageJ. (c) TiO₂ produced as a function of KSSKK concentration. The concentration of TiBALDH was held constant at 2 mM. Data are a mean of two independent repeats. (d) SEM image of SKSK₃SKS-TiO₂ coprecipitates showing spherical morphologies with a mean diameter of 511 ± 202 nm. (e) Size distribution histogram for SKSK₃SKS-TiO₂ coprecipitates. Particle sizes are measured using ImageJ. (f) TiO₂ produced as a function of SKSK₃SKS concentration. The concentration of TiBALDH was held constant at 0.1 M. Data are a mean of two independent repeats.

SKSK₃SKS embedded within the TiO₂ coprecipitate, we make site-specific ¹³C CS assignments for the entire peptide using five ¹³C-enriched samples (Table 2). Both 1D ¹³C CP MAS and

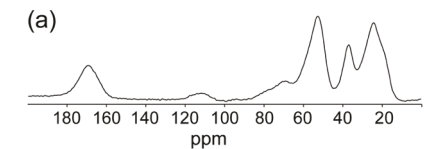
Table 2. SKSK₃SKS Samples in Which Uniformly ¹³C-Enriched Amino Acids are Incorporated

sample name	label position		
S1K2	S*K*SKKKSKS		
S3K4	SKS*K*KKSKS		
K5	SKSKK*KSKS		
K6S7	SKSKKK*SKS		
K8	SKSKKKSK*S		

2D DARR ¹³C-¹³C experiments were performed on SKSK₃SKS-neat and SKSK₃SKS-TiO₂. Figure 2 illustrates the need for 2D spectroscopy; in the 1D CP MAS NMR (Figure 2a), we are not able to resolve each shift, as there is an overlap in both the carbonyl and aliphatic regions. However, with 2D ¹³C-¹³C DARR (Figure 2b), we can resolve and assign all of the ¹³C shifts, which are provided in the Supporting Information.

Once all 13 C shifts are assigned for both the neat and TiO₂-embedded peptide, changes in backbone and side-chain CSs (Δ CS) are analyzed. 13 C CS perturbations of the backbone carbons (13 CO, 13 C α , and 13 C β) are typically associated with a change in the secondary structure, which can result from coprecipitation with TiO₂, whereas side-chain perturbations can be attributed to peptide aggregation, proximity to the TiO₂ surface, or buffer effects. To study the degree of perturbation of 13 C CSs, Δ CS values are obtained by subtracting the CS of the 13 C spin in neat SKSK₃SKS from the corresponding 13 C spin in the SKSK₃SKS-TiO₂ coprecipitate. A positive Δ CS indicates a downfield perturbation (higher ppm, less shielded), whereas a negative Δ CS indicates an upfield perturbation (lower ppm, more shielded). Bar charts of both backbone and side-chain Δ CS values are shown in Figure 3.

There are significant backbone CS perturbations upon coprecipitation with TiO₂, occurring at the S1 13 C α , S3 13 CO, K4 13 CO, K6 13 C α , S7 13 C α , and all 13 C β shifts except



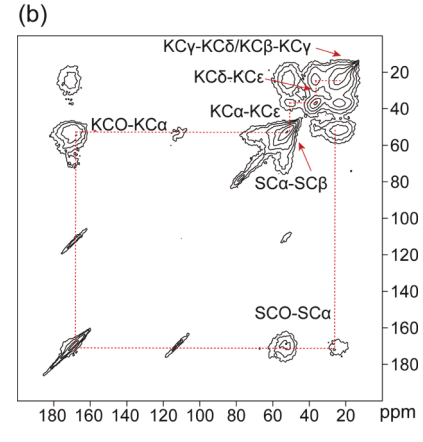


Figure 2. (a) ¹³C CP MAS NMR of SKSK₃SKS S1K2 TiO₂. (b) ¹³C-¹³C DARR of SKSK₃SKS S1K2 TiO₂. Cross peaks are labeled for ease of identification.

K6. These Δ CS values are quite large in magnitude, indicating significant structural changes in these regions, particularly around the N-terminus. There are also significant Δ CS for the side chains of SKSK₃SKS. ¹³Cγ perturbations occur at K2, K5, K6, and K8, ¹³Cδ perturbations occur at K2 and K6, and ¹³Cε perturbations occur at K8, which has a large downfield shift of 10.7 ppm.

The CS values for the 13 CO, 13 C α , and 13 C β spins are input into TALOS-N, 52 which generates output files containing predicted torsion angles (Tables S5 and S6). These torsion angles are used to visualize the secondary structure of SKSK₃SKS-neat and SKSK₃SKS-TiO₂ using Chimera, 63 as shown in Figure 4. In the neat peptide, the entire chain is extended in a random coil. However, upon coprecipitation with TiO₂, the chain kinks at K2, causing S1 and S3 to fold inward, exposing the K2 side chain. These perturbations are

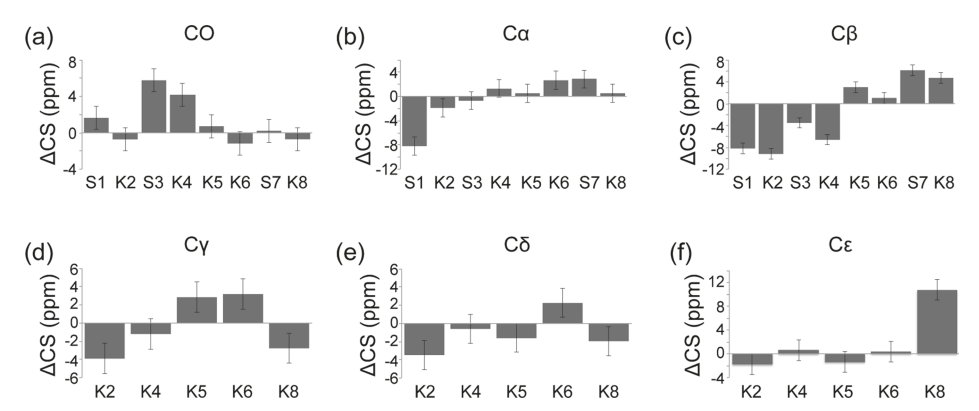


Figure 3. Δ CS plots for SKSK₃SKS showing CS perturbations for (a) 13 CO shifts, (b) 13 C α shifts, (c) 13 C β shifts, (d) 13 C γ shifts, and (f) 13 C ε shifts. Δ CS values for SKSK₃SKS coprecipitated with TiO₂ are in reference to the neat peptide. Positive changes indicate a downfield shift, whereas negative changes indicate an upfield shift.

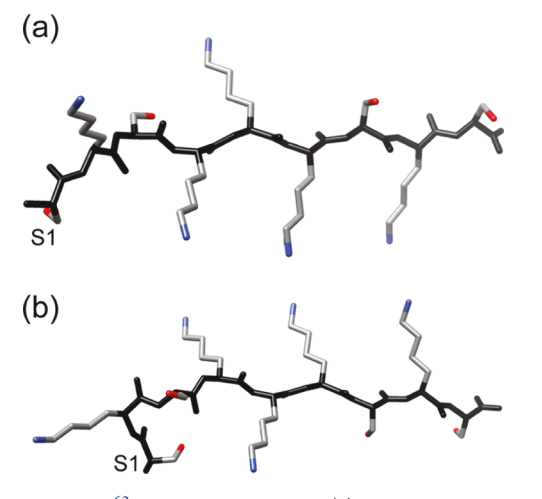


Figure 4. Chimera 63 -generated models of (a) SKSK $_3$ SKS-neat and (b) SKSK $_3$ SKS-TiO $_2$ using TALOS-N 52 —generated torsion angles from experimentally obtained CSs.

accompanied by large Δ CS for S1 backbone 13 C spins as well as K2 13 C β , 13 C γ , and 13 C δ (see Figure 3). It is interesting to note that K2 does not experience a significant Δ CS perturbation at 13 C ε . The S7 and K8 residues at the C-terminus also experience CS perturbations accompanied by structural changes, albeit more modest than those observed at S1–K3. These structural changes could result in a greater exposure of the K8 side chain, which experiences a large Δ CS at 13 C ε , a perturbation typically associated with interactions with a mineral surface. 37,57,58 In addition, the side chains of K4, K6, and K8 are all oriented on the same side of the peptide, which could be conducive to TiO₂ binding.

¹³C CS Assignments and Secondary Structure Analysis of KSSKK-Neat and KSSKK-TiO₂. Analogous to the SKSK₃SKS system, we use 1D ¹³C CP MAS and 2D DARR ¹³C–¹³C experiments to make site-specific ¹³C CS assignments (Supporting Information Tables S3 and S4) for the both the KSSKK-neat and KSSKK-TiO₂ peptides using two isotopically enriched samples (Table 3). Again, we analyze Δ CS (Figure 5) to gain insights into the structural conformations and perturbations of the neat and embedded peptides.

No significant Δ CS values are observed for any of the 13 CO spins. Many of the remaining backbone Δ CS range from 0 to 2 ppm but more significant perturbations are observed for the S2 13 C α (5.9 ppm), S2 13 C β (9.1 ppm), the S3 13 C α (4.4 ppm),

Table 3. KSSKK Samples in Which Uniformly ¹³C-Enriched Amino Acids are Incorporated

sample name	label position
K1S2	K*S*SKK
S3K4	KSS*K*K

and the K4 $^{13}\text{C}\beta$ (–2.8 ppm) shifts, indicating secondary structure changes around S2 and K4, changes that are seen in a similar region of the SKSK₃SKS peptide. In addition, there is a side-chain perturbation of –4.2 ppm in the K4 $^{13}\text{C}\delta$ shift. Interestingly, although the $^{13}\text{C}\epsilon$ of K1 shows an upfield shift of about 1 ppm, there is virtually no change in the CS of the $^{13}\text{C}\epsilon$ spin of K4 upon coprecipitation with TiO₂. This apparent difference in the surface orientations of closely spaced lysine side chains will be considered in the section on DFT calculations.

We use TALOS-N⁵² and Chimera⁵⁹ to visualize the secondary structure of KSSKK-neat and KSSKK-TiO₂, as shown in Figure 6. ϕ/ψ torsion angle values are shown in the Supporting Information (Tables S7 and S8). The N-terminus around S2 and K3 shows a mild conformational change, consistent with the observed backbone Δ CS, while the C-terminus remains relatively unchanged. The overall conformational changes upon coprecipitation with TiO₂ are minor and do not seem to alter the exposure of any side chains. This is reflected in the Δ CS, where few significant perturbations are observed in the K1 or K4 side-chain ¹³C spins, the exception being the K4 ¹³C δ shift. Perhaps because of the small size of the peptide, significant conformational changes are not required to catalyze the nucleation of TiO₂, and side chains are already oriented in a way to maximize the exposure.

DFT Calculations. The secondary structures and interactions of peptides in coprecipitates with SiO₂ have been studied extensively with ssNMR techniques. 31,37,57,58,60-62 A common approach in ssNMR studies of peptides in biosilica composites is to use heteronuclear correlation methods to directly determine peptide—SiO₂ contacts. ²⁹Si is a spin 1/2 nucleus with a natural abundance of 4.7%; ^{34,67} hence, it is frequently used in heteronuclear correlation as a target nucleus within the oxide component for recoupling to ¹³C and ¹⁵N spins in protein side chains. However, ssNMR studies of peptide—TiO₂ composites are more problematical due in part to lack of a nuclear spin within the inorganic oxide, which can serve as a target for dipolar recoupling experiments. ⁴⁷Ti and ⁴⁹Ti are both NMR-active Ti isotopes but have small

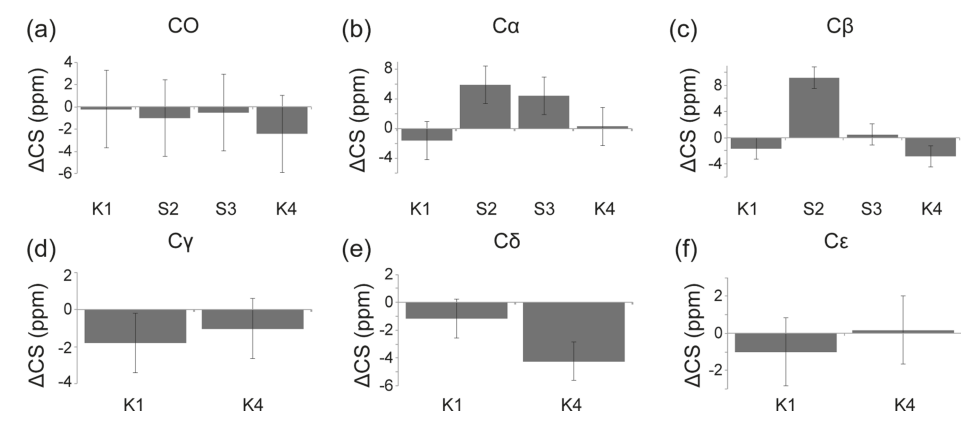


Figure 5. Δ CS plots for KSSKK showing CS perturbations for (a) 13 CO shifts, (b) 13 C α shifts, (c) 13 C β shifts, (d) 13 C γ shifts, (e) 13 C δ shifts, and (f) 13 C ϵ shifts. Δ CS values for KSSKK coprecipitated with TiO₂ are in reference to the neat peptide. Positive changes indicate a downfield shift, whereas negative changes indicate an upfield shift.

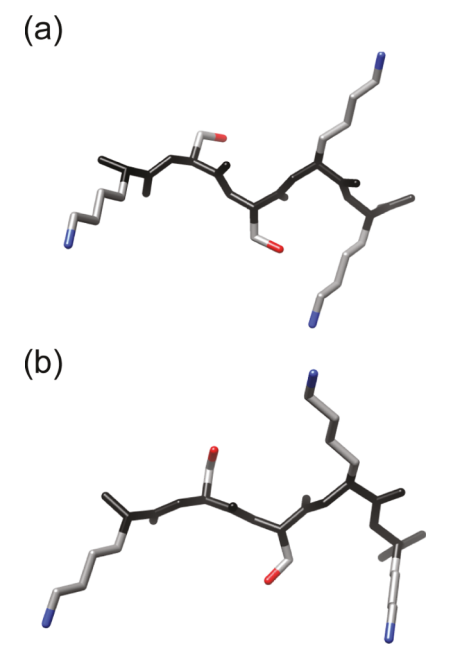


Figure 6. Chimera⁵⁹-generated models of (a) KSSKK neat and (b) KSSKK-TiO₂ using TALOS-N⁵²—generated torsion angles from experimentally obtained CSs.

gyromagnetic ratios, low natural abundances, and relatively large quadrupole moments, all resulting in low detection sensitivity. Because of these factors, direct measurements of peptide interactions with the ${\rm TiO_2}$ surface via heteronuclear dipolar recoupling experiments from spin 1/2 nuclei in protein side chains, such as $^{13}{\rm C}$ or $^{15}{\rm N}$, to $^{47}{\rm Ti}$ and $^{49}{\rm Ti}$ are not practical.

To probe peptide— TiO_2 interactions in the S–K system, we use Δ CS data obtained from 13 C spins in peptide side chains to detect changes in the electronic environment of the peptide upon coprecipitation with TiO_2 . Because TiO_2 activity is observed to scale with the number of primary amines in the R5 peptide, 21 we concentrate analysis on Δ CS effects observed for 13 C γ , 13 C δ , and 13 C ε spins of lysine side chains. We assume however that Δ CS effects in peptide—inorganic oxide composites can have a number of origins; hence, to clarify the physical circumstances that give rise to these side-chain CS perturbations, we use DFT calculations. Protein side chains may undergo conformational changes when adapting to mineral

surfaces. Table 4 shows the compiled DFT calculations of CS changes for lysine side chain 13 C γ , 13 C δ , and 13 C ε spins that

Table 4. Influence of Lysine Side-Chain Conformation on the CSs of the ${}^{13}\text{C}\gamma$, ${}^{13}\text{C}\delta$, and ${}^{13}\text{C}\varepsilon$ Spins (ppm) a

	γ-60	γ60	δ-60	$\delta 60$	ε-60	ε60
Сγ	-3.53	0.95	-0.64	-0.75	-0.74	-0.84
$C\delta$	-3.18	-2.77	-1.07	-0.99	-1.29	-1.27
$C\varepsilon$	0.48	0.37	-0.77	-0.60	0.62	0.54

"Positive table entries indicate downfield CS perturbations with respect to the all trans conformation.

result from the conformational changes of the side chain. In Table 4, $\gamma \pm 60$ indicates a change of the $C\alpha C\beta - C\gamma C\delta$ dihedral angle by $\pm 60^{\circ}$. Similarly, $\delta \pm 60$ and $\varepsilon \pm 60$ indicate $\pm 60^{\circ}$ changes of the $C\beta C\gamma - C\delta C\varepsilon$ and $C\gamma C\delta - C\varepsilon N\zeta$ dihedral angles, respectively. (All entries are in ppm, with positive numbers indicating downfield CS changes and negative numbers indicating upfield CS changes relative to the all-trans side-chain conformation.)

In ssNMR studies of surface adsorbed amino acids and peptides, upfield perturbations of lysine side-chain ^{13}C CSs (i.e. $\Delta CS < 0$), and $^{13}C\varepsilon$ in particular, have been attributed to the interactions with negative charges in mineral surfaces. 57,58 Recently, Guo and Holland used a combination of ssNMR and DFT calculations to elucidate the adsorption state of lysine on fumed silica surfaces. 68 They modeled the interaction of lysine with the silica surface as a lysine—silanol complex and calculated ^{15}N and ^{13}C CSs for lysine free and in the complex. On the basis of a comparison between calculated and experimental CSs, it was concluded that the lysine amine is the dominant hydrogen bonding interaction with the surface silanol groups. 68

To address the possibility that lysine amines in KSSKK and SKSK₃SKS similarly form interactions with hydroxyl groups in peptide—TiO₂ composites, DFT calculations of lysine side-chain ¹³C CS perturbations were performed for varying distances between the side-chain amine nitrogen and the nearest surface hydroxyl oxygen. These calculations were made for two side-chain orientations relative to the TiO₂ surface. Results are shown in Figure 7. Figure 7a shows chemical shift perturbations as a function of distance between amine nitrogen and surface hydroxyl oxygen for a perpendicular alignment of the lysine side chain relative to the TiO₂ surface. For this

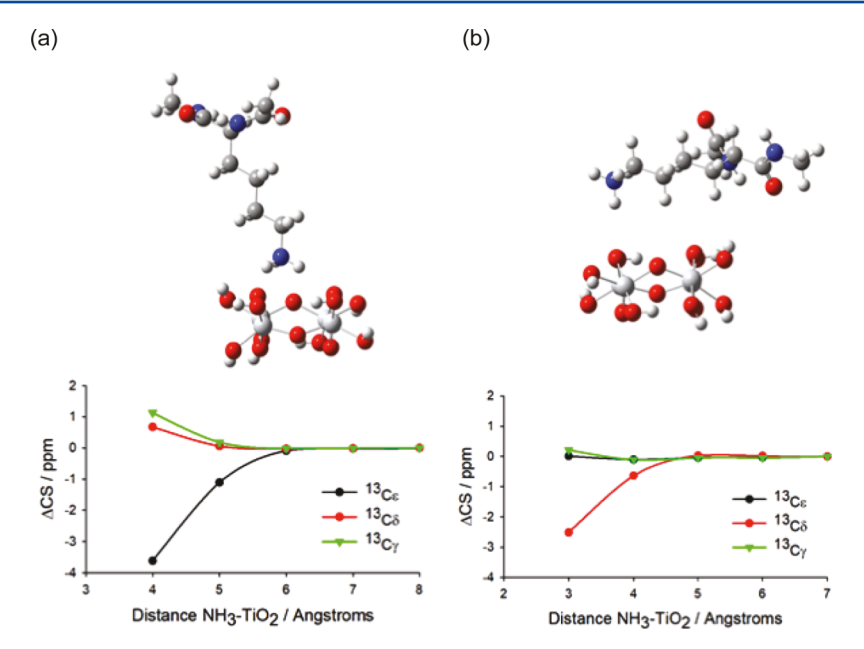


Figure 7. DFT calculation of lysine side-chain 13 C CS perturbations (Δ CS) as a function of the distance between the lysine amine nitrogen and the surface hydroxyl oxygen for (a) a perpendicular orientation of the lysine side chain relative to the TiO₂ surface and (b) a parallel orientation of the lysine side chain relative to the TiO₂ surface. An upfield perturbation of a 13 C CS is indicated by Δ CS < 0 and a downfield perturbation is therefore indicated by Δ CS > 0.

surface orientation, a DFT calculation shows a 2-3 ppm upfield perturbation of the 13CE CS and weaker downfield perturbations of the 13 C γ and 13 C δ CSs when the amine N to surface hydroxyl O distance approaches 4 Å Figure 7b shows Δ CS effects calculated for 13 C spins in a lysine side chain that approaches a TiO2 surface in a parallel orientation. The parallel orientation is much less conducive to hydrogen bond formation between the lysine side-chain amine and surface hydroxyl groups. Accordingly, the DFT calculations in Figure 7b show that the pattern of ΔCS effects in the parallel side-chain orientation differs markedly from the pattern observed for the perpendicular side-chain orientation in Figure 7a. The most significant difference is that the 2-3 ppm upfield shift of the $^{13}\text{C}\varepsilon$ spin observed in the perpendicular orientation is not observed for the parallel orientation. In contrast, the parallel orientation shows modest downfield shifts for the ¹³Cγ and $^{13}\text{C}\varepsilon$ spins while the $^{13}\text{C}\delta$ spin shows large upfield shifts. The upfield shift observed for the ${}^{13}\text{C}\delta$ spin is due to the proximity of the ${}^{1}H\delta$ spin to the TiO₂ surface, although the 2.5 ppm upfield shift corresponding to a N-O distance of 3 Å is somewhat too small for an H-bond interaction. For a more realistic N–O distance of 3.8–4.0 Å, the upfield shift for 13 C δ is calculated to be in the range 0.5-1.0 ppm.

DISCUSSION

¹³CO, ¹³Cα, and ¹³Cβ CS data indicate both S–K peptides SKSK₃SKS and KSSKK are in extended secondary structures in the neat form and largely remain in extended structures in TiO₂ composites. Significant Δ CS effects observed for ¹³CO, ¹³Cα, and ¹³Cβ spins are confined to the termini of both the SKSK₃SKS and KSSKK peptides. For the KSSKK system, perturbations of the ¹³Cα and ¹³Cβ of S2 are accompanied by a small conformational change at S2–K4 as well as a Δ CS for ¹³Cδ of K4. It is possible that the structural rearrangement at S2–K4 acts to better orient the side chain of K4 for interactions with the TiO₂ surface.

The pattern of side-chain ¹³C CS perturbations in K1 differs from the pattern observed in K4. For K1, the CS of $^{13}C\varepsilon$ is perturbed upfield by about 1 ppm (i.e., $\Delta CS = -1$ ppm) and the CS of 13 C δ is also perturbed upfield by about 1 ppm, while the upfield perturbation of 13 C γ is somewhat larger at about 1.8 ppm. In the case of ${}^{13}\text{C}\varepsilon$, the $\Delta\text{CS} = -1$ ppm is in the range expected for a N-O distance of about 4-5 Å, assuming the side-chain approaches the TiO2 surface with the threefold symmetry axis of the side-chain amine group directed perpendicular to the surface as shown in Figure 7. On the other hand, the upfield Δ CS effects observed at 13 C γ and 13 C δ for K1 do not agree with what is expected if the lysine side chain maintains an all-trans conformation when oriented with the amine group directed toward the TiO2 surface as shown in Figure 7a. The upfield Δ CS effects observed at 13 C γ and 13 C δ are likely due to a conformational change of the side chain as it approaches the TiO₂ surface.

In the case of K4, the $^{13}C\varepsilon$ CS is only weakly perturbed while 1–4 ppm upfield Δ CS effects are observed at $^{13}C\gamma$ and $^{13}C\delta$. The negligible change in the CS of $^{13}C\varepsilon$ precludes a close association with the TiO_2 surface at least not in the orientation assumed in the DFT calculations shown in Figure 7a. The fact that both $^{13}C\delta$ and $^{13}C\gamma$ are shifted upfield precludes an orientation of the type shown in Figure 7b. This pattern of Δ CS effects likely indicates the conformational change of the K4 side chain upon coprecipitation with TiO_2 , possibly involving a change of the $C\alpha C\beta - C\gamma C\delta$ dihedral angle in the range $\pm 60^\circ$, which would exert only a small downfield change in the CS of $^{13}C\varepsilon$.

CS trends observed for the five lysine side chains in SKSK₃SKS indicate a more complex interaction with the TiO_2 mineral phase than is the case with KSSKK. Δ CS trends for 13 CO, 13 C α , and 13 C β in the S1–K4 region indicate a backbone conformational change upon coprecipitation with TiO_2 , but the rest of the backbone maintains an extended secondary structure. The Δ CS values observed for the 13 C ε , 13 C δ , and 13 C γ spins in the five lysine side chains vary. For example, upon

coprecipitation with TiO_2 , the side chain of $K2^{13}C\varepsilon$ is shifted upfield by about 2 ppm ($\Delta CS = -2$ ppm) while $^{13}C\delta$ and $^{13}C\gamma$ show upfield CS perturbations of about 3–3.5 ppm. The upfield perturbation of the $^{13}C\varepsilon$ CS again very likely indicates an interaction with the TiO_2 surface. Assuming an orientation as shown in Figure 7a, the observed ca. 2 ppm upfield shift corresponds to a N–O distance of about 4.5 Å. The 3–3.5 ppm upfield CS perturbations observed for the $^{13}C\gamma$ and $^{13}C\delta$ spins in K2 may be due to a conformational change of the side chain, most likely a ca. 60° change of the $C\alpha C\beta - C\gamma C\delta$ dihedral angle.

The Δ CS trends observed for $^{13}\text{C}\gamma/^{13}\text{C}\delta/^{13}\text{C}\varepsilon$ in K4 differ markedly from those observed in K2. Δ CS effects are small for both $^{13}\text{C}\varepsilon$ and $^{13}\text{C}\delta$ with a 1.0 ppm upfield shift of $^{13}\text{C}\gamma$. At K5, the CS of $^{13}\text{C}\varepsilon$ changes in the upfield direction by 2.0 ppm (Δ CS = -2.0 ppm) upon coprecipitation with TiO₂, and a change of the CSs of $^{13}\text{C}\delta$ and $^{13}\text{C}\gamma$ by -1 and 2 ppm, respectively. K6 shows a small change in the CS of $^{13}\text{C}\varepsilon$ upon coprecipitation with TiO₂, while both $^{13}\text{C}\gamma$ and $^{13}\text{C}\delta$ show downfield shifts of between 2 and 3 ppm. The trend in K8 is different still with $^{13}\text{C}\gamma$ and $^{13}\text{C}\delta$ showing upfield CS perturbations in the 2-3 ppm range upon coprecipitation with TiO₂ while $^{13}\text{C}\varepsilon$ shows a large downfield shift.

Although the ¹³C CS data are not conclusive with regard to the nature of interactions between SKSK₃SKS and TiO₂, DFT calculations reported in this work and experimental and computational studies reported elsewhere indicate that lysine side chains interact strongly with TiO₂ surfaces. 43,69,70 Therefore, it is not surprising that in many cases upfield perturbations are observed for ¹³Cε spins in SKSK₃SKS peptide-TiO₂ coprecipitates. However, if the SKSK₃SKS peptides were dispersed as monomers within a matrix of TiO2, it might be expected that the ${}^{13}\text{C}\varepsilon$ spins would experience similar electronic environments, and in such cases, all lysine side chains would display CS trends of the types shown in Figure 7. However, in the SKSK₃SKS peptide, the CS perturbations observed for 13 C ε spins in the lysine side chains vary considerably with K2 and K5 showing upfield perturbations expected for side chains in close proximity to TiO2 surfaces with perpendicular orientations, while K4 and K6 show only weak perturbations, indicating that these spins are remote from the surface or deviate from the perpendicular orientation. The large downfield perturbation to the CS of ${}^{13}\text{C}\varepsilon$ in K8 is striking because none of the DFT results in Table 4 or Figure 7 account for the significant downfield shifts for lysine side-chain ¹³C spins. Downfield perturbations of side-chain spins have been observed in peptide-silica composites and have been attributed to peptide-peptide aggregation. 22,34,40,64-66

The self-assembly of high phosphorylated silaffins has been observed and proposed as a mechanism for catalyzing silica formation. The self-assembly hypothesis has been extended to the silaffin-derived peptide R5 to explain its SiO_2 forming and TiO_2 forming activities. The Δ CS data obtained in this study do not provide direct proof of the existence of SK peptide aggregates in TiO_2 composites, but in our recent solid-state NMR study of the R5 peptide in SiO_2 and TiO_2 composites, the variation in lysine side-chain CS perturbations is suggestive of differential exposure of the protein side chains to TiO_2 which in turn may be the result of the self assembly of the monomeric peptides into aggregates which persist in the solid composite.

This interpretation of the ΔCS data for the two peptides is supported by DFT calculations and also by the precipitation curves Figure 1. In Figure 1c, the precipitation curve of KSSKK is hyperbolic in form, with the TiO_2 -peptide composite

precipitating at extremely low concentrations of peptide before reaching saturation at a peptide concentration of about 2 mM. In contrast, the precipitation curve for SKSK₃SKS, shown in Figure 1f, is sigmoidal, with no appreciable amounts of precipitate forming until a peptide concentration of 2 mM is reached. The curve for SKSK₃SKS saturates at about 8 mM. The higher activity of SKSK₃SKS is not surprising given the larger number of K residues, but the different curve shapes requires explanation. Various factors have been discussed as the causes for variation in peptide isotherm curve shapes. For example, adsorption isotherms for small peptides onto negatively charged silica surfaces differ markedly for cationic versus anionic or uncharged peptides, with the cationic peptides adsorbing at low concentrations onto silica particles at higher levels than the anionic or neutral peptides at similar concentrations.⁷² Given that both peptides in this study are cationic, the difference in the precipitation curves of KSSKK and SKSK₃SKS may be better explained by other mechanisms, including the occurrence of an equilibrium between monomeric peptides and peptide aggregates. 73,74 In cases where interactions between peptide side chains and inorganic oxide precursors compete with peptide-peptide interactions, sigmoidality of the isotherm is favored by higher populations of aggregate versus monomer, whereas hyperbolic behavior is favored by higher populations of monomer.⁷⁴ Also in selfaggregating systems, if aggregation does not result in a loss of peptide sites (lysine side chains) for interacting with oxide precursors, hyperbolic behavior is approached as the affinities of precursor for monomer and polymer become equivalent. Departures from hyperbolic behavior increase as interactions between precursors and monomer and aggregate become inequivalent. Therefore, a plausible explanation for the difference between the precipitation curves of KSSKK and SKSK₃SKS is the existence of a monomer-aggregate equilibrium, where the populations of the monomer versus aggregate differ between the two peptide samples, where affinities of oxide precursors for sites on the monomer versus aggregate may differ between the two samples and where precursor-peptide interactions compete with peptide-peptide interactions. The latter condition would require that the sites on the peptide for interactions with precursors are close to or identical to the sites for peptide-peptide interactions.

CONCLUSIONS

Although S–K peptides have been reported earlier to induce silica formation from solutions of silicic acid, this is the first study of S–K peptides as catalysts for the mineralization of a nonbiological oxide, that is, TiO₂. This study has assayed a series of S–K peptides of varying lengths, primary structures, K–S ratios, and TiO₂ precipitation activities. Two of these peptides (SKSK₃SKS and KSSKK) have similar K–S ratios but different lengths and display very different precipitation activities but produce similar TiO₂ morphologies, albeit with different particle size distributions. In addition, precipitation curves differ markedly; the curve for KSSKK has a hyperbolic form, and the curve for SKSK₃SKS displays a sigmoidal form.

Unlike silica or hydroxyapatite, ${\rm TiO_2}$ lacks a nuclear spin species which can be incorporated into heteronuclear dipolar correlation experiments; hence, quantitative determination of distances between $^{13}{\rm C}$ and $^{15}{\rm N}$ spins in peptide side chains to spins in the oxide surface via dipolar interactions is impractical. Instead, in this study, the sensitivity of CSs of lysine side chain $^{13}{\rm C}$ spins to charged oxide surfaces has been used in place of

dipolar recoupling experiments to determine peptide-surface proximity and orientation. Qualitative trends in ΔCS of side chain spins observed upon coprecipitation with TiO_2 have been quantified using DFT computations and have enabled interpretation of side chain spin ΔCS trends in terms of changes in peptide side-chain conformation, orientation, and proximity to TiO_2 surfaces.

For both peptides, upfield shifts for some lysine $^{13}C\varepsilon$ spins indicate contact between the mineral. However, in both peptides, some ${}^{13}\text{C}\varepsilon$ spins show little CS perturbation or, in the case of lysine side chains near the C-terminus in SKSK₃SKS, show downfield perturbations. These results indicate that the peptide side chains are not uniformly exposed to the mineral but are possibly in aggregated states, which may as a result remove some side chains from close contact with the mineral surface. Recent ssNMR studies indicate that R5 may similarly aggregate in the presence of phosphate to form TiO2 from TiBALDH solutions.²² That KSSKK shows a hyperbolic precipitation curve may indicate that this peptide has a lower population of aggregate versus monomer than is the case with SKSK₃SKS, although there are alternative explanations of such peptide-peptide and peptide-TiBALDH interactions occurring independently⁷⁴ while these interactions may occur competitively in SKSK₃SKS. If the CS patterns observed for the S-K peptides in this study indicate that these peptides similarly aggregate in the course of forming TiO2, then they do so in the absence of phosphate. The nature of peptide-peptide interactions in these composite systems is the subject of future studies.

ASSOCIATED CONTENT

S Supporting Information

The Supporting Information is available free of charge on the ACS Publications website at DOI: 10.1021/acs.jpcb.8b00745.

Process of peptide design and tables of all ¹³C CS assignments and torsion angles (PDF)

AUTHOR INFORMATION

Corresponding Author

*E-mail: drobny@chem.washington.edu.

ORCID ®

Gary P. Drobny: 0000-0002-7293-1897

Notes

The authors declare no competing financial interest.

ACKNOWLEDGMENTS

Part of this work was conducted at the Molecular Analysis Facility, which is supported in part by funds from the Molecular Engineering and Sciences Institute, the Clean Energy Institute, the National Science Foundation grants CHE-1219509. G.P.D. acknowledges support from NSF MCB—1715123 and U.S. Army contract W911QY-13-2-0004v. M.D. acknowledges support from the Czech Science Foundation (grant 18-11851S).

REFERENCES

- (1) Fujishima, A.; Honda, K. Electrochemical Photolysis of Water at a Semiconductor Electrode. *Nature* **1972**, 238, 37–38.
- (2) Hoffmann, M. R.; Martin, S. T.; Choi, W.; Bahnemann, D. W. Environmental Applications of Semiconductor Photocatalysis. *Chem. Rev.* **1995**, *95*, *69*–*96*.

- (3) Linsebigler, A. L.; Lu, G.; Yates, J. T. Photocatalysis on TiO2 Surfaces: Principles, Mechanisms, and Selected Results. *Chem. Rev.* **1995**, *95*, 735–758.
- (4) Abo-Farha, S. A. Photocatalytic Degradation of Monoazo and Diazo Dyes in Wastewater on Nanometer-Sized TiO2. *J. Am. Sci.* **2010**, *6*, 130–142.
- (5) Acevedo, A.; Carpio, E. A.; Rodríguez, J.; Manzano, M. A. Disinfection of Natural Water by Solar Photocatalysis Using Immobilized TiO2 Devices: Efficiency in Eliminating Indicator Bacteria and Operating Life of the System. *J. Sol. Energy Eng.* **2012**, *134*, 011008.
- (6) Adachi, M.; Murata, Y.; Wang, F.; Jiu, J. Synthesis of Titania Nanocrystals: Application for Dye-Sensitized Solar Cells. *Self-Organized Nanoscale Materials*; Springer: New York, NY, 2006; pp 71–100.
- (7) Varghese, O. K.; Grimes, C. A. Metal Oxide Nanoarchitectures for Environmental Sensing. *J. Nanosci. Nanotechnol.* **2003**, *3*, 277–293.
- (8) Wintermantel, E.; Eckert, K.-L.; Huang, N.-P.; Textor, M.; Brunette, D. M. *Titanium Ceramics for Cell-Carriers and for Medical Applications*; Springer: Berlin Heidelberg, 2001; pp 649–671.
- (9) Chen, X.; Mao, S. S. Titanium Dioxide Nanomaterials: Synthesis, Properties, Modifications, and Applications. *Chem. Rev.* **2007**, *107*, 2891–2959.
- (10) Madden, T. H.; Datye, A. K.; Fulton, M. Oxidation of Metal-EDTA Complexes by TiO 2 Photocatalysis. *Environ. Sci. Technol.* **1997**, *31*, 3475–3481.
- (11) Huang, M.; Tso, E.; Datye, A. K.; Prairie, M. R.; Stange, B. M. Removal of Silver in Photographic Processing Waste by TiO 2 -Based Photocatalysis. *Environ. Sci. Technol.* **1996**, *30*, 3084–3088.
- (12) Prairie, M. R.; Evans, L. R.; Stange, B. M.; Martinez, S. L. An Investigation of Ti02 Photocatalysis for the Treatment of Water Contaminated with Metals and Organic Chemicals. *Environ. Sci. Technol.* **1993**, *27*, 1776–1782.
- (13) Zhang, Z.; Wang, C.-C.; Zakaria, R.; Ying, J. Y. Role of Particle Size in Nanocrystalline TiO 2 -Based Photocatalysts. *J. Phys. Chem. B* **1998**, *102*, 10871–10878.
- (14) Qian, Y.; Chen, Q.; Chen, Z.; Fan, C.; Zhou, G. Preparation of Ultrafine Powders of TiO2, by Hydrothermal H202 Oxidation Starting from Metallic Ti. *J. Mater. Chem.* **1993**, *3*, 203–205.
- (15) Chhabra, V.; Pillai, V.; Mishra, B. K.; Morrone, A.; Shah, D. O. Synthesis, Characterization, and Properties of Microemulsion-Mediated Nanophase Ti02 Particles. *Langmuir* 1995, 11, 3307–3311.
- (16) Cheng, H.; Ma, J.; Zhao, Z.; Qi, L. Hydrothermal Preparation of Uniform Nanosize Rutile and Anatase Particles. *Chem. Mater.* **1995**, *7*, 663–671.
- (17) Jang, H. D.; Kim, S.-K. Controlled Synthesis of Titanium Dioxide Nanoparticles in a Modified Diffusion Flame Reactor. *Mater. Res. Bull.* **2001**, *36*, 627–637.
- (18) Maslova, M. V.; Rusanova, D.; Naydenov, V.; Antzutkin, O. N.; Gerasimova, L. G. Extended Study on the Synthesis of Amorphous Titanium Phosphates with Tailored Sorption Properties. *J. Non-Cryst. Solids* **2012**, *358*, 2943–2950.
- (19) Dickerson, M. B.; Sandhage, K. H.; Naik, R. R. Protein- and Peptide-Directed Syntheses of Inorganic Materials. *Chem. Rev.* **2008**, 108, 4935–4978.
- (20) Chen, C.-L.; Rosi, N. L. Peptide-Based Methods for the Preparation of Nanostructured Inorganic Materials. *Angew. Chem., Int. Ed.* **2010**, 49, 1924–1942.
- (21) Sewell, S. L.; Wright, D. W. Biomimetic Synthesis of Titanium Dioxide Utilizing the R5 Peptide Derived from Cylindrotheca Fusiformis. *Chem. Mater.* **2006**, *18*, 3108–3113.
- (22) Buckle, E. L.; Roehrich, A.; Vandermoon, B.; Drobny, G. P. Comparative Study of Secondary Structure and Interactions of the R5 Peptide in Silicon Oxide and Titanium Oxide Coprecipitates Using Solid-State NMR Spectroscopy. *Langmuir* 2017, 33, 10517–10524.
- (23) Kröger, N.; Deutzmann, R.; Bergsdorf, C.; Sumper, M. Species-Specific Polyamines from Diatoms Control Silica Morphology. *Proc. Natl. Acad. Sci. U. S. A.* **2000**, *97*, 14133–14138.

- (24) Kröger, N.; Deutzmann, R.; Sumper, M. Silica-Precipitating Peptides from Diatoms The Chemical Structure Of Silaffin-1A from Cylindrotheca Fusiformis. *J. Biol. Chem.* **2001**, *276*, 26066–26070.
- (25) Lopez, P.; Gautier, C.; Livage, J.; Coradin, T. Mimicking Biogenic Silica Nanostructures Formation. *Curr. Nanosci.* **2005**, *1*, 73–83
- (26) Hildebrand, M.; Dahlin, K.; Volcani, B. E. Characterization of a Silicon Transporter Gene Family in Cylindrotheca Fusiformis: Sequences, Expression Analysis, and Identification of Homologs in Other Diatoms. MGG, Mol. Gen. Genet. 1998, 260, 480–486.
- (27) Hildebrand, M. Diatoms, Biomineralization Processes, and Genomics. *Chem. Rev.* **2008**, *108*, 4855–4874.
- (28) Kröger, N.; Poulsen, N. Diatoms-from Cell Wall Biogenesis to Nanotechnology. *Annu. Rev. Genet.* **2008**, *42*, 83–107.
- (29) Naik, R. R.; Whitlock, P. W.; Rodriguez, F.; Brott, L. L.; Glawe, D. D.; Clarson, S. J.; Stone, M. O. Controlled Formation of Biosilica Structures in Vitro. *Chem. Commun.* **2003**, 238–239.
- (30) Knecht, M. R.; Wright, D. W. Functional Analysis of the Biomimetic Silica Precipitating Activity of the R5 Peptide from Cylindrotheca Fusiformis. *Chem. Commun.* **2003**, 3038–3039.
- (31) Lechner, C. C.; Becker, C. F. W. Modified Silaffin R5 Peptides Enable Encapsulation and Release of Cargo Molecules from Biomimetic Silica Particles. *Bioorg. Med. Chem.* **2013**, *21*, 3533–3541.
- (32) Senior, L.; Crump, M. P.; Williams, C.; Booth, P. J.; Mann, S.; Perriman, A. W.; Curnow, P. Structure and Function of the Silicifying Peptide RS. J. Mater. Chem. B 2015, 3, 2607–2614.
- (33) Poulsen, N.; Scheffel, A.; Sheppard, V. C.; Chesley, P. M.; Kröger, N. Pentalysine Clusters Mediate Silica Targeting of Silaffins in Thalassiosira Pseudonana. *J. Biol. Chem.* **2013**, 288, 20100–20109.
- (34) Geiger, Y.; Gottlieb, H. E.; Akbey, Ü.; Oschkinat, H.; Goobes, G. Studying the Conformation of a Silaffin-Derived Pentalysine Peptide Embedded in Bioinspired Silica Using Solution and Dynamic Nuclear Polarization Magic-Angle Spinning NMR. *J. Am. Chem. Soc.* **2016**, *138*, 5561–5567.
- (35) Li, N.; Zhang, X.; Wang, Q.; Wang, F.; Shen, P. Biomimetic Synthesis of Silica Hollow Spheres Using Poly (L-Lysine) and Mechanism Research. *RSC Adv.* **2012**, *2*, 3288–3297.
- (36) van Bommel, K. J. C.; Jung, J. H.; Shinkai, S. Poly(L-Lysine) Aggregates as Templates for the Formation of Hollow Silica Spheres. *Adv. Mater.* **2001**, *13*, 1472–1476.
- (37) Mizutani, T.; Nagase, H.; Ogoshi, H. Silicic Acid Polymerization Catalyzed by Amines and Polyamines. *Chem. Lett.* **1998**, 133–134.
- (38) Cole, K. E.; Valentine, A. M. Spermidine and Spermine Catalyze the Formation of Nanostructured Titanium Oxide. *Biomacromolecules* **2007**, *8*, 1641–1647.
- (39) Sumper, M.; Lorenz, S.; Brunner, E. Biomimetic Control of Size in the Polyamine-Directed Formation of Silica Nanospheres. *Angew. Chem., Int. Ed.* **2003**, *42*, 5192–5195.
- (40) Zane, A. C.; Michelet, C.; Roehrich, A.; Emani, P. S.; Drobny, G. P. Silica Morphogenesis by Lysine-Leucine Peptides with Hydrophobic Periodicity. *Langmuir* **2014**, *30*, 7152–7161.
- (41) Kang, S.-J.; Won, H.-S.; Choi, W.-S.; Lee, B.-J. De Novo Generation of Antimicrobial LK Peptides with a Single Tryptophan at the Critical Amphipathic Interface. *J. Pept. Sci.* **2009**, *15*, 583–588.
- (42) DeGrado, W. F.; Lear, J. D. Induction of Peptide Conformation at Apolar Water Interfaces. 1. A Study with Model Peptides of Defined Hydrophobic Periodicity. *J. Am. Chem. Soc.* **1985**, *107*, 7684–7689.
- (43) Sano, K.-I.; Sasaki, H.; Shiba, K. Specificity and Biomineralization Activities of Ti-Binding Peptide-1 (TBP-1). *Langmuir* **2005**, *21*, 3090–3095.
- (44) Durupthy, O.; Bill, J.; Aldinger, F. Bioinspired Synthesis of Crystalline TiO2: Effect of Amino Acids on Nanoparticles Structure and Shape. *Cryst. Growth Des.* **2007**, *7*, 2696–2704.
- (45) Dickerson, M. B.; Jones, S. E.; Cai, Y.; Ahmad, G.; Naik, R. R.; Kröger, N.; Sandhage, K. H. Identification and Design of Peptides for the Rapid, High-Yield Formation of Nanoparticulate TiO 2 from Aqueous Solutions at Room Temperature. *Chem. Mater.* **2008**, *20*, 1578–1584.

- (46) Fang, Y.; Wu, Q.; Dickerson, M. B.; Cai, Y.; Shian, S.; Berrigan, J. D.; Poulsen, N.; Kröger, N.; Sandhage, K. H. Protein-Mediated Layer-by-Layer Syntheses of Freestanding Microscale Titania Structures with Biologically Assembled 3-D Morphologies. *Chem. Mater.* **2009**, *21*, 5704–5710.
- (47) Kharlampieva, E.; Jung, C. M.; Kozlovskaya, V.; Tsukruk, V. V. Secondary Structure of Silaffin at Interfaces and Titania Formation. *J. Mater. Chem.* **2010**, 20, 5242–5250.
- (48) Hernández-Gordillo, A.; Hernández-Arana, A.; Campero, A.; Vera-Robles, L. I. Biomimetic Sol—Gel Synthesis of TiO 2 and SiO 2 Nanostructures. *Langmuir* **2014**, *30*, 4084–4093.
- (49) Kröger, N.; Sandhage, K. H. From Diatom Biomolecules to Bioinspired Syntheses of Silica-and Titania-Based Materials Silica Formation In Vitro Using Biomolecules from Diatoms. *MRS Bull.* **2010**, 35, 122–126.
- (50) Sultan, A. M.; Hughes, Z. E.; Walsh, T. R. Binding Affinities of Amino Acid Analogues at the Charged Aqueous Titania Interface: Implications for Titania-Binding Peptides. *Langmuir* **2014**, *30*, 13321–13329
- (51) Stote, R. E.; Filocamo, S. F.; Lum, J. S. Silaffin Primary Structure and Its Effects on the Precipitation Morphology of Titanium Dioxide. *J. Mater. Res.* **2016**, *31*, 1373–1382.
- (52) Shen, Y.; Bax, A. Protein Backbone and Sidechain Torsion Angles Predicted from NMR Chemical Shifts Using Artificial Neural Networks. *J. Biomol. NMR* **2013**, *56*, 227–241.
- (53) Yoe, J. H.; Armstrong, A. R. Colorimetric Determination of Titanium with Disodium-1,2-Dihydroxybenzene-3,5-Disulfonate. *Anal. Chem.* **1947**, *19*, 100–102.
- (54) Puddu, V.; Slocik, J. M.; Naik, R. R.; Perry, C. C. Titania Binding Peptides as Templates in the Biomimetic Synthesis of Stable Titania Nanosols: Insight into the Role of Buffers in Peptide-Mediated Mineralization. *Langmuir* **2013**, *29*, 9464–9472.
- (55) Takegoshi, K.; Nakamura, S.; Terao, T. 13C-1H Dipolar-Assisted Rotational Resonance in Magic-Angle Spinning NMR. *Chem. Phys. Lett.* **2001**, 344, 631–637.
- (56) Morcombe, C. R.; Zilm, K. W. Chemical Shift Referencing in MAS Solid State NMR. J. Magn. Reson. 2003, 162, 479–486.
- (57) Becke, A. D. Density-functional Thermochemistry. III. The Role of Exact Exchange. *J. Chem. Phys.* **1993**, 98, 5648–5652.
- (58) Lee, C.; Yang, W.; Parr, R. G. Development of the Colle-Salvetti Correlation-Energy Formula into a Functional of the Electron Density. *Phys. Rev. B: Condens. Matter Mater. Phys.* **1988**, *37*, 785–789.
- (59) Barone, V.; Cossi, M. Quantum Calculation of Molecular Energies and Energy Gradients in Solution by a Conductor Solvent Model. *J. Phys. Chem. A* **1998**, *102*, 1995–2001.
- (60) Cossi, M.; Rega, N.; Scalmani, G.; Barone, V. Energies, Structures, and Electronic Properties of Molecules in Solution with the C-PCM Solvation Model. *J. Comput. Chem.* **2003**, *24*, 669–681.
- (61) Frisch, M. J.; Trucks, G. W.; Schlegel, H. B.; Scuseria, G. E.; Robb, M. A.; Cheeseman, J. R.; Scalmani, G.; Barone, V.; Petersson, G. A.; Nakatsuji, H.; et al. *Gaussian 16*, Revision A.03; Gaussian, Inc: Wallingford, CT, 2016.
- (62) Rueden, C.; Dietz, C.; Horn, M.; Schindelin, J.; Northan, B.; Berthold, M.; Eliceiri, K. *ImageJ Ops*, 2016.
- (63) Pettersen, E. F.; Goddard, T. D.; Huang, C. C.; Couch, G. S.; Greenblatt, D. M.; Meng, E. C.; Ferrin, T. E. UCSF Chimera A Visualization System for Exploratory Research and Analysis. *J. Comput. Chem.* **2004**, *25*, 1605–1612.
- (64) Fernandez, V. L.; Reimer, J. A.; Denn, M. M. Magnetic Resonance Studies of Polypeptides Adsorbed on Silica and Hydroxyapatite Surfaces. *J. Am. Chem. Soc.* **1992**, *114*, 9634–9642.
- (65) Roehrich, A.; Drobny, G. Solid-State NMR Studies of Biomineralization Peptides and Proteins. *Acc. Chem. Res.* **2013**, *46*, 2136–2144.
- (66) Shir, I. B.; Kababya, S.; Amitay-Rosen, T.; Balazs, Y. S.; Schmidt, A. Molecular Level Characterization of the Inorganic-Bioorganic Interface by Solid State NMR: Alanine on a Silica Surface, a Case Study. *J. Phys. Chem. B* **2010**, *114*, 5989–5996.

- (67) Wisser, D.; Brückner, S. I.; Wisser, F. M.; Althoff-Ospelt, G.; Getzschmann, J.; Kaskel, S.; Brunner, E. 1H-13C-29Si Triple Resonance and REDOR Solid-State NMR- A Tool to Study Interactions between Biosilica and Organic Molecules in Diatom Cell Walls. *Solid State Nucl. Magn. Reson.* **2015**, 66–67, 33–39.
- (68) Guo, C.; Holland, G. P. Investigating Lysine Adsorption on Fumed Silica Nanoparticles. *J. Phys. Chem. C* **2014**, *118*, 25792–25801.
- (69) Hayashi, T.; Sano, K.-I.; Shiba, K.; Iwahori, K.; Yamashita, I.; Hara, M. Critical Amino Acid Residues for the Specific Binding of the Ti-Recognizing Recombinant Ferritin with Oxide Surfaces of Titanium and Silicon. *Langmuir* **2009**, *25*, 10901–10906.
- (70) Suzuki, Y.; Shindo, H.; Asakura, T. Structure and Dynamic Properties of a Ti-Binding Peptide Bound to TiO ₂ Nanoparticles As Accessed by ¹ H NMR Spectroscopy. *J. Phys. Chem. B* **2016**, *120*, 4600–4607.
- (71) Kröger, N.; Lorenz, S.; Brunner, E.; Sumper, M. Self-Assembly of Highly Phosphorylated Silaffins and Their Function in Biosilica Morphogenesis. *Science* **2002**, *298*, 584–586.
- (72) Patwardhan, S. V.; Emami, F. S.; Berry, R. J.; Jones, S. E.; Naik, R. R.; Deschaume, O.; Heinz, H.; Perry, C. C. Chemistry of Aqueous Silica Nanoparticle Surfaces and the Mechanism of Selective Peptide Adsorption. *J. Am. Chem. Soc.* **2012**, *134*, 6244–6256.
- (73) Fournier, N. C.; Rahim, M. H. Self-Aggregation, a New Property of Cardiac Fatty Acid-Binding Protein Predictable Influence on Energy Production in the Heart. *J. Biol. Chem.* **1983**, 258, 2929–2933.
- (74) Nichol, L. W.; Jackson, W. J. H.; Winzor, D. J. A Theoretical Study of the Binding of Small Molecules to a Polymerizing Protein System. A Model for Allosteric Effects. *Biochemistry* **1967**, *6*, 2449–2456.